Electronic Supplementary Information

Highly pH–stable lanthanide MOFs: tunable luminescence and ratiometric luminescent probe for sulfamethazine

Xu Zhang,[a] Dongyan Liu,[a] Jiahui Yu,[a] Xin Li,[a] Hanwen Zheng,[a] Yanan Zhou,[a] Cuiying Huang,*[a] Yanyu Zhu,[a] Chengqi Jiao*[ab] and Zhengang Sun*[a]

[a]*School of Chemistry and Chemical Engineering, Liaoning Normal University, Dalian 116029, P. R. China*

[b]*State Key Laboratory of Fine Chemicals, Dalian University of Technology, Dalian 116024, P. R. China.*

E–mail: huangcy0828@126.com, jiaochengqi1989@163.com, szg188@163.com

CONTENTS:

Experimental section

Materials and measurements. All reagents and solvents were purchased from commercial suppliers and utilized without further purification. The diphosphonic acid H_4L was prepared according to the literature reported previously. [S1] Elemental analyses (C, H and N) were performed on a PE−2400 elemental analyzer. IR spectra were measured using a Bruker AXS TENSOR–27 FT–IR spectrometer from 4000 to 400 cm^{-1}. Thermogravimetric analyses (TG) were performed using a PerkinElmer Pyris Diamond TG–DTA thermal analyses system in the range of 50–1250 °C with a heating rate of 10 °C min^{-1}. Powder X–ray diffraction (PXRD) pattern was conducted on a Bruker AXS D8 ADVANCE diffractometer with Cu Kα radiation. UV–vis spectra were measured on a Lambda 35 spectrophotometer. Luminescent spectra were measured using a HITACHIF–7000 spectrofluorimeter. Luminescent lifetime was recorded on a HORIBA Scientifc FluoroMax–4 TCSPC spectrofluorometer. The highest occupied molecular orbital (HOMO) and the lowest unoccupied molecular orbital (LUMO) energy levels of H_4L ligand and SMZ were calculated by the density functional theory (DFT) method at the B3LYP/6–31G*(d) level in the Gaussian 09 program package.[S2]

X-ray crystallographic. Data collections for **1**–**3** were achieved on a Bruker AXS Smart APEX II CCD X–diffractometer with graphite–monochromated Mo Kα (λ = 0.71073 Å) at 296(2) K. The Olex 2 program was used to solve the structures by direct methods and refined on F^2 by full–matrix least–squares methods.[S3] All non–H atoms were refined with anisotropic thermal parameters. The H atoms except those of

water molecules were generated geometrically with fixed isotropic thermal parameters. A summary of the crystallographic data and refinement parameters are listed in Table S1. Bond distances and angles of **1**–**3** are provided in Table S2–S4.

Luminescent sensing experiments. As for the sensing experiments of common urine chemicals, 2.0 mg of **3** powder was immersed into the 3.0 mL aqueous solution (1.0×10^{-3} M), including different urine chemicals of NaCl, KCl, NH_4Cl, Na_2SO_4, Urea, Glucose, Creatine, Creatinine, and SMZ followed by ultrasonication for approximately 15 min, and then obtained the stable suspensions. Luminescent spectra of the suspensions were collected. Then, the luminescent spectra of the **3** suspensions (2.0 mg **3** in 3.0 mL deionized water after treating by ultrasonication for 15 min) were measured in situ after incremental addition of freshly prepared SMZ solutions (0–0.338 mM). After each addition, the luminescent spectrum of the suspension was monitored. **3** shows a linear tendency in the quenching process, the luminescent quenching efficiency can be quantitatively explained by the linear Stern–Volmer (S–V) equation (1), and the limits of detection (LODs) were calculated by the equation (2):

$$SD = \sqrt{\frac{1}{N-1}\sum_{I=1}\left(F - F_0\right)^2} \quad (1)$$

$$LOD = \frac{3SD}{|S|} \quad (2)$$

where *SD* is the standard deviation of replicate detection of blank solutions (N = 10), *F* is the relative luminescent intensities (I_L/I_{Tb}), F_0 is the average of *F* and *S* is the slope of the linear relationship in Fig. 5b.

Recyclable luminescence experiments. The solid powder of **3** after sensing SMZ was centrifuged for 10 minutes, then, washed the solid powder three times with water, filter and dry, and then the sample was used for the next cycle experiment. The same operation was performed five times.

Sensing of SMZ in real samples of urine and mariculture water. In order to verify the detection effectiveness of **3** in real samples, human urine and mariculture water were collected for the sensing experiments. A human urine sample (10 mL) was collected from a healthy volunteer and was stored at 4 °C immediately after collection. The sample was centrifuged for 15 min when used, the supernatant was then filtered using a 0.22–μm filter and then diluted 1000 times with deionized water for analysis. The mariculture water sample (10 mL) was collected from Malan River in Dalian. s. The prepared solution was added into complex assemblies **3**/SMZ to measure fluorescence spectra, and the fluorescence recovery efficiency $[(F_2–F_1)/ F_1]$ was calculated at each concentration. Standard addition method was used for the determination of SMZ in real sample.

Methods for preparing inks: Gel ink pens (0.5 mm) were utilized in this research. The ink barrel was first washed with water to remove the original ink. Then, the ink barrel and nib were cleaned completely in an ultrasonic bath with ethanol. The ink was prepared by adding 50 mg of **1**, **3**, **5**, and **6** powder to 25 mL mixed solvent (including 45% ethanol, 45% ethylene glycol, 5% glycerol, and 5% diethylene glycol), and then 75 mg sodium dodecyl sulfonate powder was added into the above system and ultrasonic was carried out for 10 minutes, then the mixed ink was injected to the

gel pen with a microinjector.

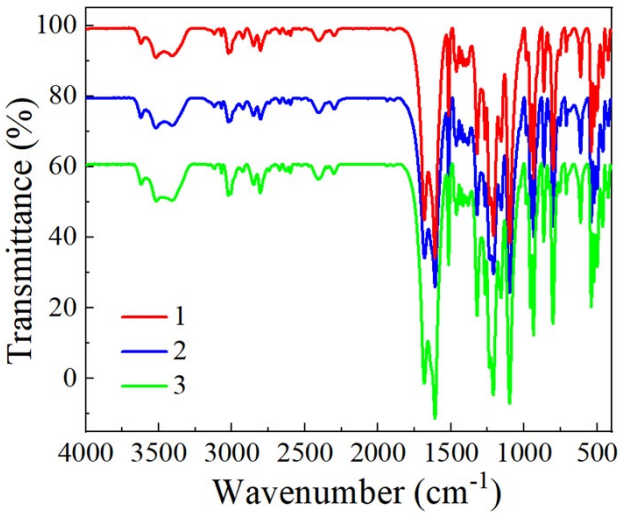

Fig. S1. IR spectra of **1–3**.

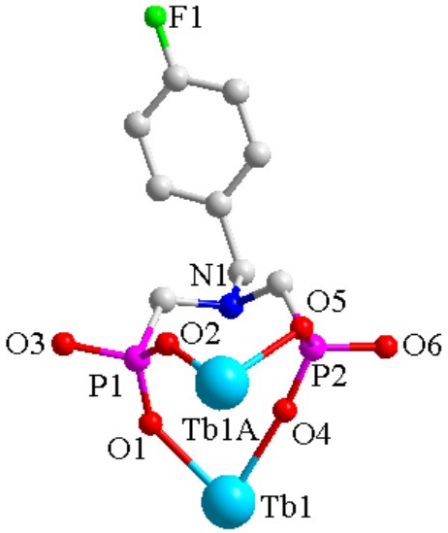

Fig. S2. Coordination mode of the H_4L ligand in **3**.

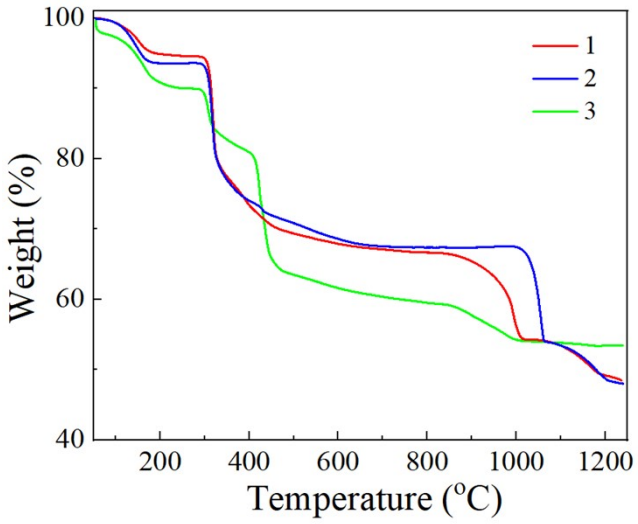

Fig. S3. TG curves of **1–3**.

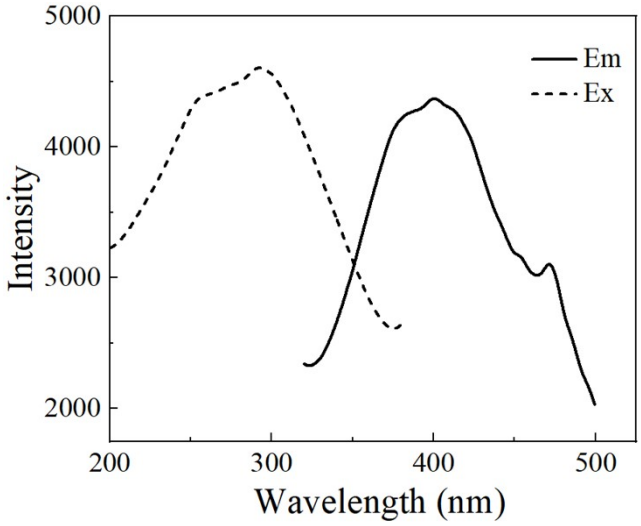

Fig. S4. Solid–state luminescent spectra of H_4L.

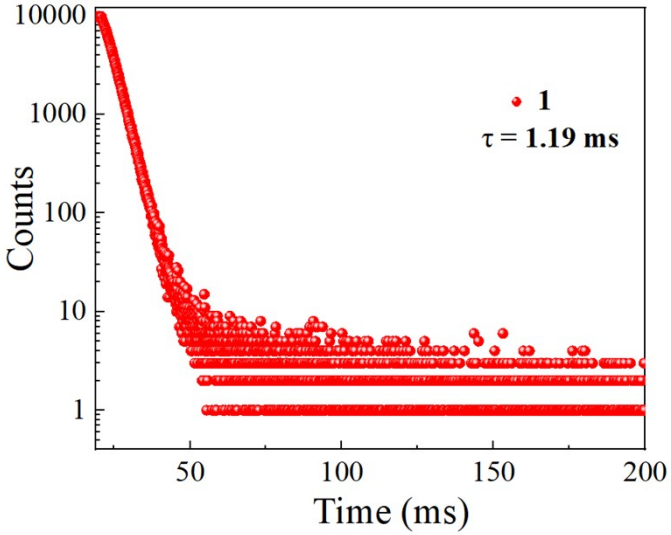

Fig. S5. Emission decay profile of **1**.

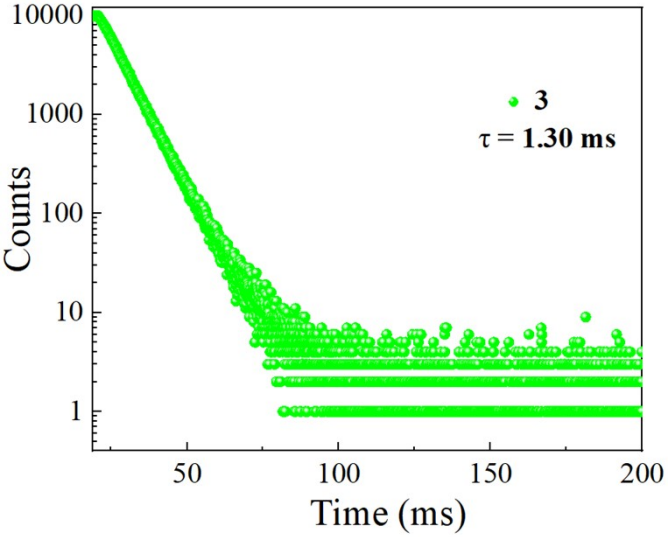

Fig. S6. Emission decay profiles of **3**.

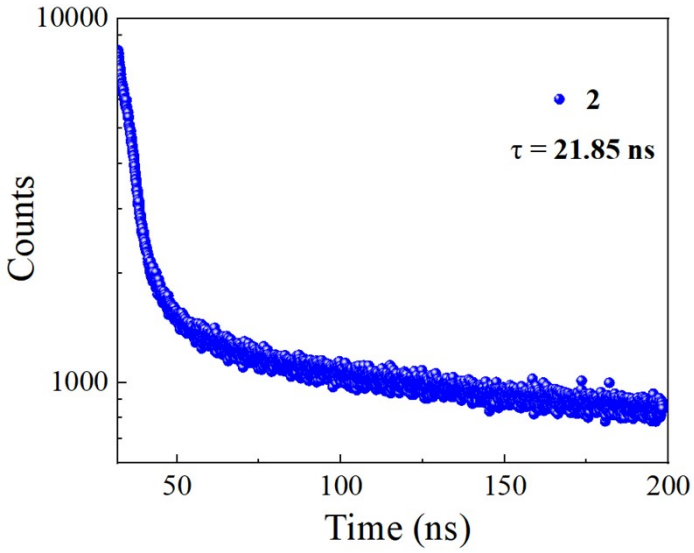

Fig. S7. Emission decay profiles of **2**.

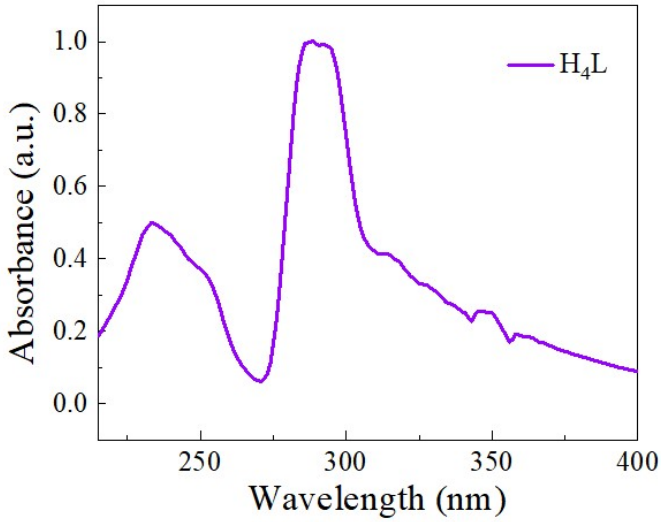

Fig. S8. UV–Vis absorption spectrum of H_4L.

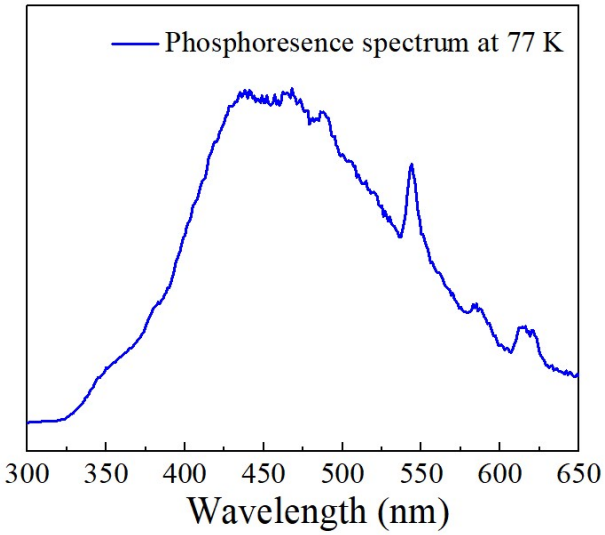

Fig. S9. Phosphorescence spectrum of **2** at 77 K.

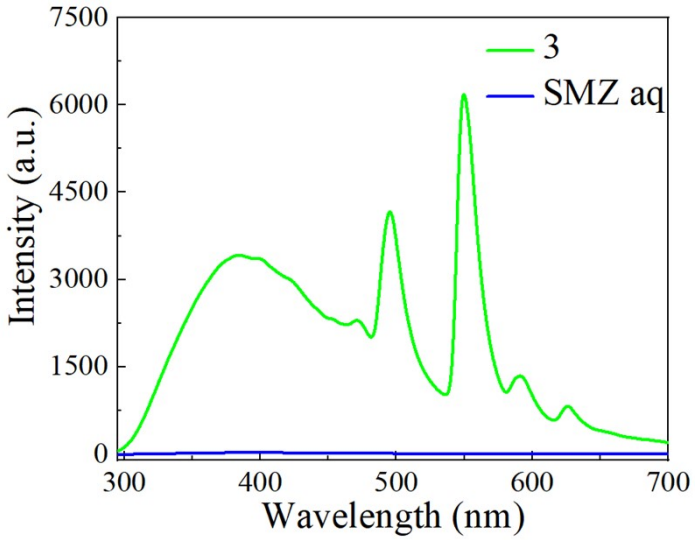

Fig. S10. Luminescent spectra of **3** and SMZ in aqueous solution.

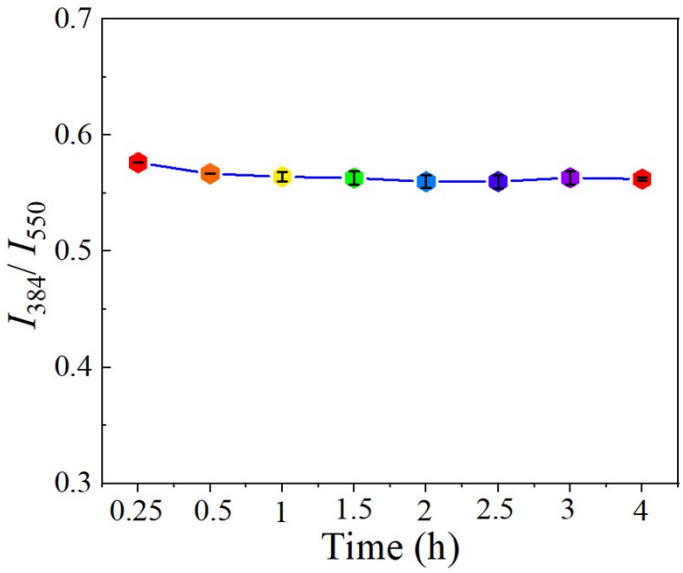

Fig. S11. The intensity ratio I_{384}/I_{550} of **3** in aqueous solutions within 4 h.

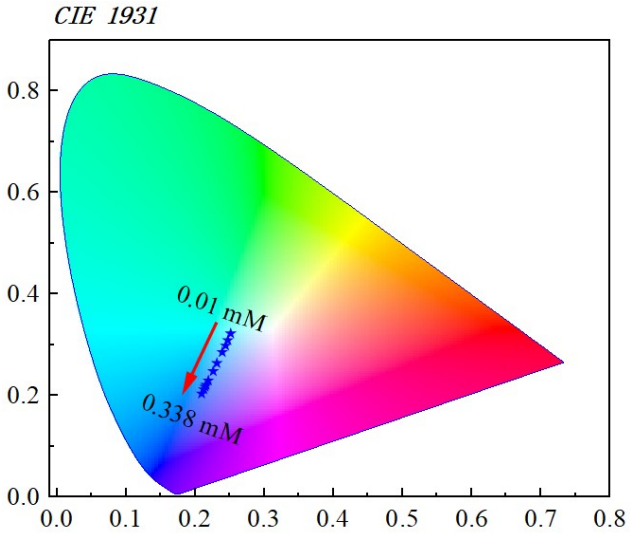

Fig. S12. CIE chromaticity diagram showing the variation of fluorescent color coordinates of the **3** dispersions in different SMZ concentrations (0–0.338 mM).

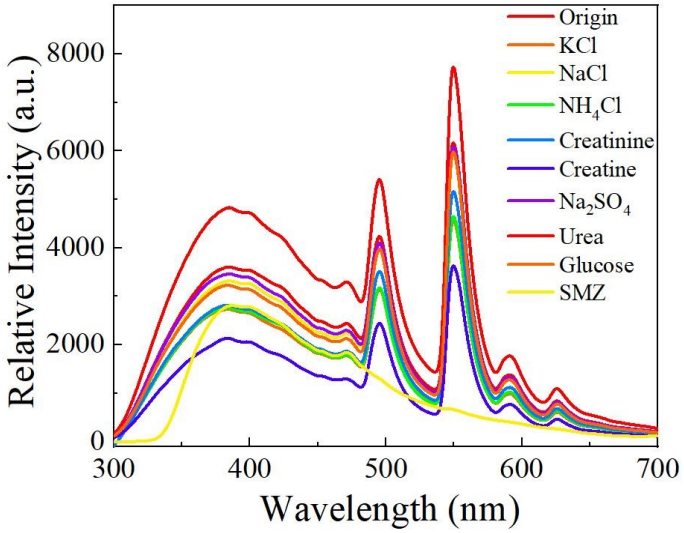

Fig. S13. Luminescent spectra of **3** suspensions with various urine components.

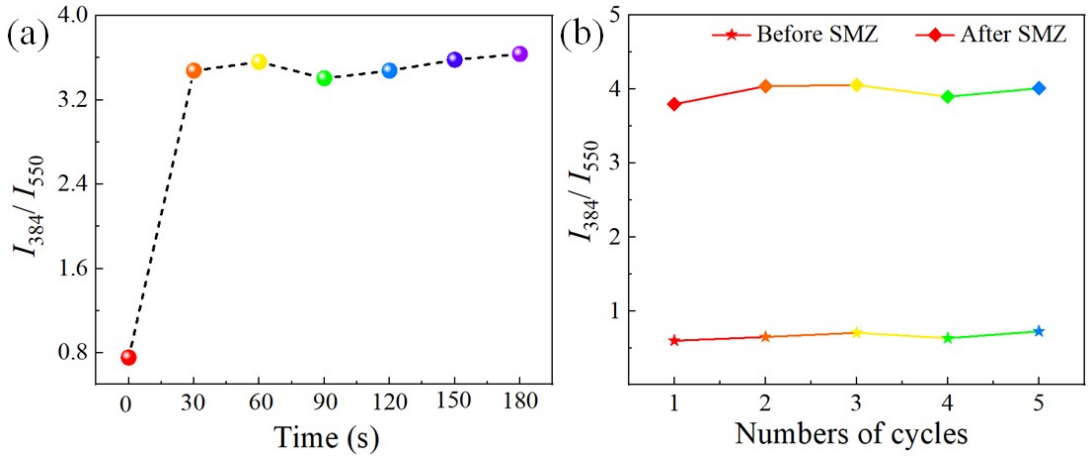

Fig. S14. (a) The relative intensities of I_{384}/I_{550} of **3** after the addition of SMZ at different times; (b) The recyclable study of **3** towards SMZ.

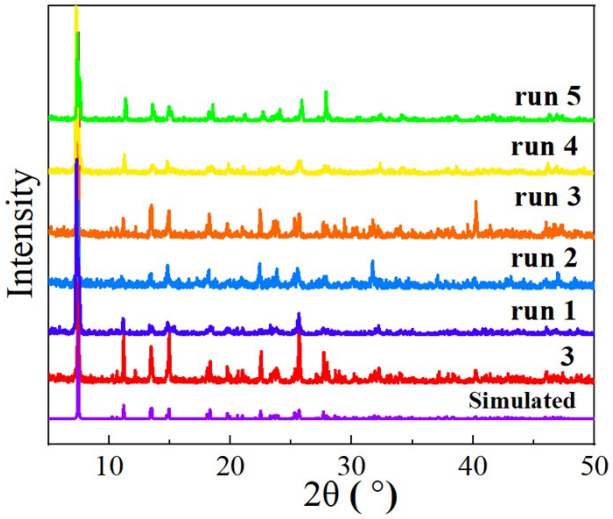

Fig. S15. PXRD patterns of **3** after five recycles of sensing for SMZ aqueous solution.

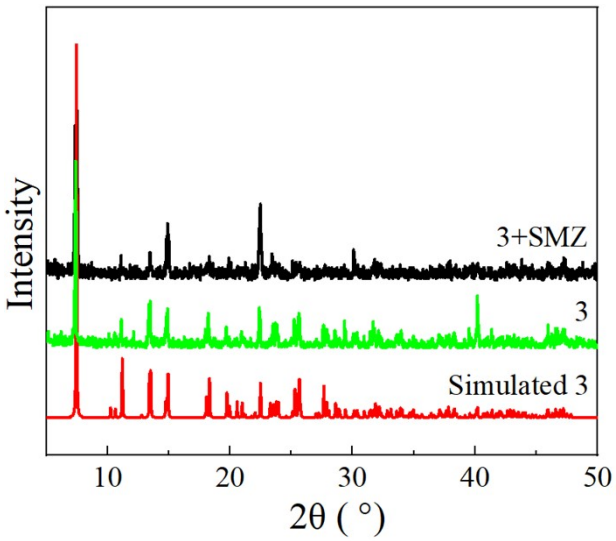

Fig. S16. PXRD patterns of **3** before and after detection of SMZ.

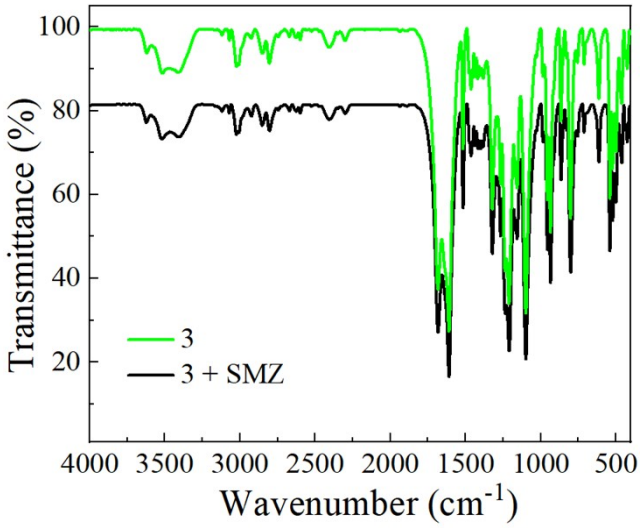

Fig. S17. IR spectra of **3** before and after detection of SMZ.

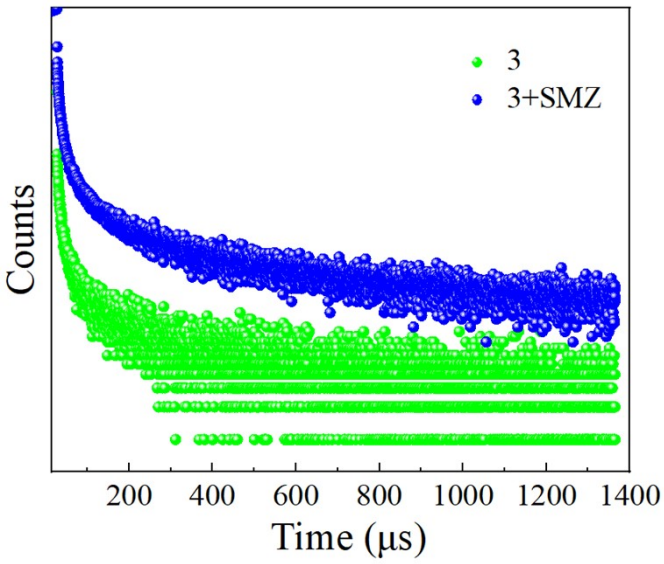

Fig. S18. Emission decay profiles of **3** suspensions before and after sensing of SMZ.

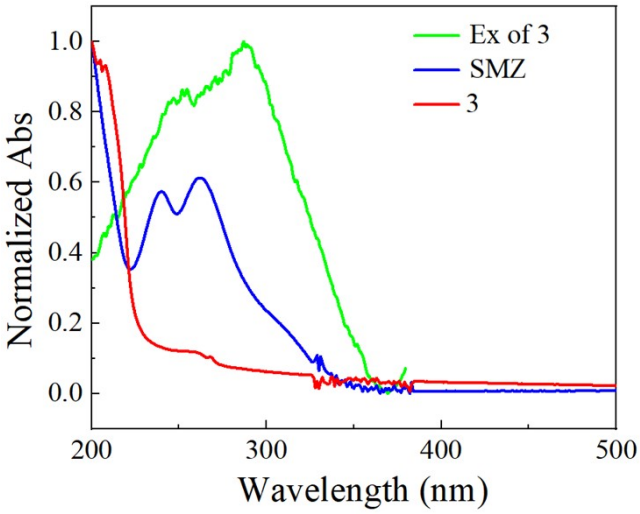

Fig. S19. UV−vis absorption spectra of **3**, SMZ and excitation spectrum of **3** in aqueous solutions.

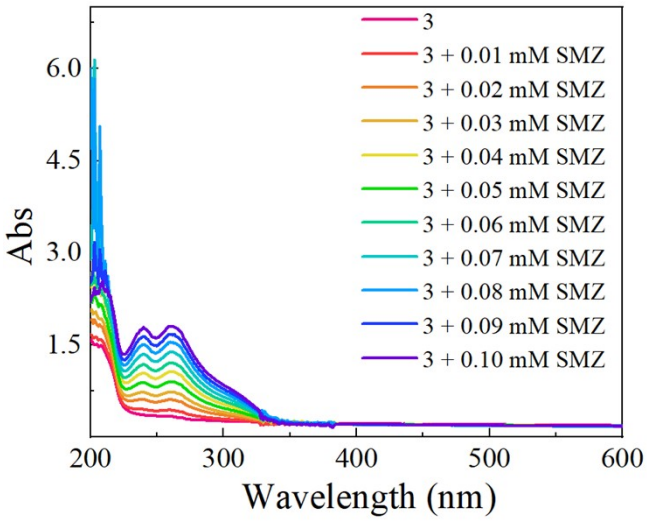

Fig. S20. UV–vis spectra of **3** in the presence of various concentrations (0–0.099 mM) of SMZ solutions.

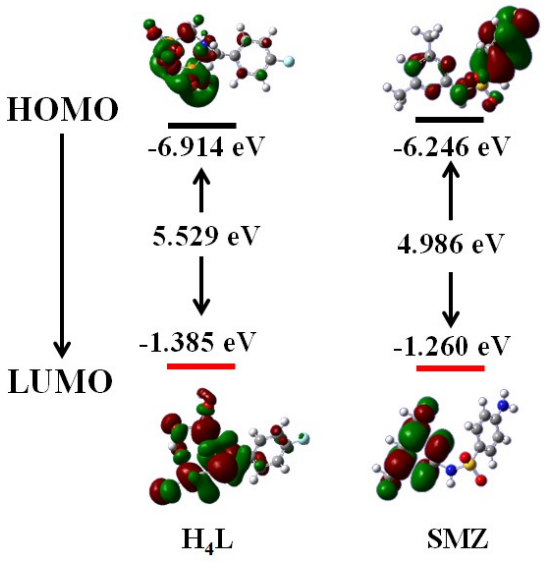

Fig. S21. HOMO and LUMO energy levels of the SMZ and the H_4L calculated by density functional theory (DFT) at B3LYP/6–31G*(d) basis set.

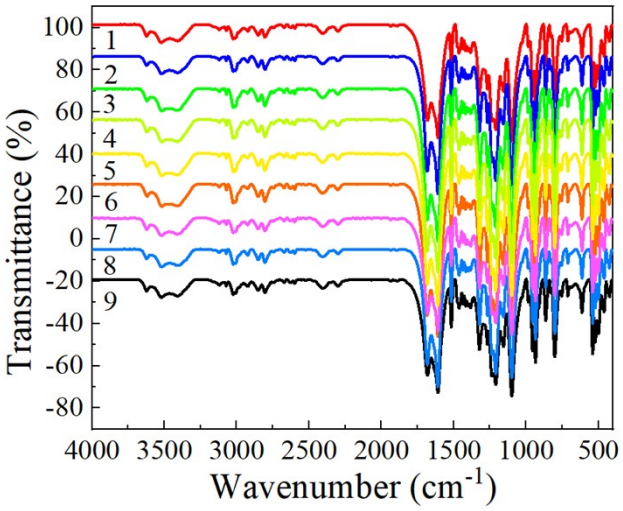

Fig. S22. IR spectra of **1–9.**

Table S1. Crystal data and structure refinements for **1–3**.

Compounds	**1**	**2**	**3**
Empirical formula	$C_{11}H_{17}EuFNO_{12}P_2$	$C_{11}H_{17}FGdNO_{12}P_2$	$C_{11}H_{17}FNO_{12}P_2Tb$
Formula weight	588.15	594.45	595.11
Crystal system	Monoclinic	Monoclinic	Monoclinic
Space group	C2/c	C2/c	C2/c
a/Å	28.970(3)	29.012(4)	29.0892(16)
b/Å	8.9096(8)	8.8924(13)	8.8694(5)
c/Å	17.3086(15)	17.275(2)	17.2574(9)
α/°	90	90	90
β/°	125.3620(10)	125.362(2)	125.399(5)
γ/°	90	90	90
V/Å^3	3643.3(6)	3634.5(9)	3629.4(4)
Z	8	8	8
ρ_{calc}g/cm^3	2.145	2.173	2.178
μ/mm^{-1}	3.693	3.900	4.148
F(000)	2304.0	2320.0	2320.0
Reflections collected	11349	12162	8555
Independent reflections	4434 [R_{int} = 0.0481]	4965 [R_{int} = 0.0382]	3130 [R_{int} = 0.0778]
Completeness	100%	100%	97%
Goodness of fit on F^2	0.989	0.984	1.050
[a]R_1, wR_2 [$I>2\sigma(I)$]	0.0339, 0.0558	0.0310, 0.0611	0.0750, 0.1450
[a]R_1, wR_2 (all data)	0.0599, 0.0616	0.0492, 0.0670	0.0934, 0.1536

[a] $R_1 = \Sigma\,(|F_0|-|F_C|) / \Sigma\,|F_0|$; $wR_2 = [\Sigma\, w\,(|F_0|-|F_C|)^2 / \Sigma\, w\, F_0^2]^{1/2}$

Table S2. Selected bond lengths (Å) and angles (º) for **1.**

Eu1–O4	2.337(3)
Eu1–O9#1	2.459(3)
Eu1–O10#1	2.493(3)
Eu1–O1	2.437(3)
Eu1–O2#2	2.376(3)
Eu1–O7	2.451(3)
Eu1–O5#2	2.335(3)
Eu1–O8	2.459(3)
O4–Eu1–O9#1	79.28(10)
O4–Eu1–O10#1	136.87(10)
O4–Eu1–O1	74.69(10)
O4–Eu1–O2#2	78.35(10)
O4–Eu1–O7	82.86(10)
O4–Eu1–O8	143.03(10)
O9#1–Eu1–O10#1	65.69(10)
O1–Eu1–O9#1	139.23(10)
O1–Eu1–O10#1	148.29(10)
O1–Eu1–O7	76.56(10)
O1–Eu1–O8	79.00(10)
O2#2–Eu1–O9#1	79.46(10)
O2#2–Eu1–O10#1	71.44(10)
O2#2–Eu1–O1	123.94(10)
O2#2–Eu1–O7	146.13(10)
O2#2–Eu1–O8	138.53(10)
O7–Eu1–O9#1	69.46(10)
O7–Eu1–O10#1	105.96(10)
O7–Eu1–O8	65.93(10)
O5#2–Eu1–O4	124.09(10)
O5#2–Eu1–O9#1	140.33(10)
O5#2–Eu1–O10#1	77.27(10)
O5#2–Eu1–O1	80.41(11)
O5#2–Eu1–O2#2	75.64(10)
C11–O9–Eu1#3	119.9(3)
C10–O10–Eu1#3	118.4(3)

Symmetry transformations used to generate equivalent atoms:
#1 1/2–x, 1/2+y, 1/2–z; #2 1/2–x, 3/2–y, 1–z; #3 1/2–x, –1/2+y, 1/2–z.

Table S3. Selected bond lengths (Å) and angles (º) for **2.**

Gd1–O8	2.435(3)
Gd1–O4	2.366(3)
Gd1–O10#1	2.449(3)
Gd1–O9#1	2.481(3)
Gd1–O7	2.452(3)
Gd1–O1	2.324(3)
Gd1–O2#2	2.331(3)
Gd1–O6#2	2.420(3)
O1–Gd1–O4	75.69(9)
O1–Gd1–O10#1	140.86(9)
O1–Gd1–O9#1	77.71(9)
O1–Gd1–O7	75.49(9)
O1–Gd1–O2#2	123.24(9)
O1–Gd1–O6#2	79.61(10)
O2#2–Gd1–O8	83.12(9)
O2#2–Gd1–O4	78.13(9)
O2#2–Gd1–O10#1	79.37(9)
O2#2–Gd1–O9#1	137.04(9)
O2#2–Gd1–O6#2	74.68(9)
O6#2–Gd1–O8	76.85(9)
O6#2–Gd1–O10#1	139.52(9)
O6#2–Gd1–O9#1	148.06(9)
O6#2–Gd1–O7	79.06(9)
O4–P2–O5	109.41(16)
O4–P2–O6	116.37(16)
C9–O10–Gd1#3	119.4(2)
C10–O9–Gd1#3	118.6(2)

Symmetry transformations used to generate equivalent atoms:
#1 1/2–x, 1/2+y, 3/2–z; #2 1/2–x, 1/2–y, 1–z; #3 1/2–x, –1/2+y, 3/2–z.

Table S4. Selected bond lengths (Å) and angles (º) for **3.**

Tb1–O2#1	2.354(9)
Tb1–O1	2.404(10)
Tb1–O5#1	2.318(10)
Tb1–O4	2.312(10)
Tb1–O7	2.471(10)
Tb1–O8	2.463(10)
Tb1–O9#2	2.452(10)
Tb1–O10#2	2.437(10)
O2#1–Tb1–O1	123.9(3)
O2#1–Tb1–O7	71.5(3)
O2#1–Tb1–O8	79.1(3)
O2#1–Tb1–O9#2	138.4(3)
O2#1–Tb1–O10#2	146.0(3)
O1–Tb1–O7	148.0(4)
O1–Tb1–O8	139.2(4)
O1–Tb1–O9#2	79.0(3)
O1–Tb1–O10#2	76.5(3)
O5#1–Tb1–O2#1	75.4(4)
O5#1–Tb1–O1	79.9(4)
O5#1–Tb1–O7	77.6(3)
O5#1–Tb1–O8	140.9(4)
O5#1–Tb1–O9#2	75.7(3)
O5#1–Tb1–O10#2	138.3(4)
O4–Tb1–O2#1	78.3(3)
O4–Tb1–O1	74.8(4)
O4–Tb1–O5#1	123.3(3)
O4–Tb1–O7	137.1(3)
O4–Tb1–O8	78.8(3)
O4–Tb1–O9#2	143.2(3)
O4–Tb1–O10#2	82.6(3)
O2#1–Tb1–O1	123.9(3)
O2#1–Tb1–O7	71.5(3)
O2#1–Tb1–O8	79.1(3)
O2#1–Tb1–O9#2	138.4(3)
O2#1–Tb1–O10#2	146.0(3)
O1–Tb1–O7	148.0(4)
C10–O9–Tb1#3	118.1(10)
C11–O10–Tb1#3	119.0(10)

Symmetry transformations used to generate equivalent atoms:

#1 1/2–x, 3/2–y, –z; #2 1/2–x, 1/2+y, 1/2–z; #3 1/2–x, –1/2+y, 1/2–z.

Table S5. Comparison of the proposed sensor for SMZ detection with other methods.

Sensing Method	Material	K_{sv}/M^{-1}	LOD	Visual detection	Ref.
SPE–spectrophotometric	SDB–RPS/DMCA	–	0.024 μM	No	S4
Fluorescent aptasensor	SMZ1S–AuNPs–RhoB	–	0.003 ng mL^{-1}	No	S5
SERS	PVA–CD–Ag hydrogel	–	0.036 ng mL^{-1}	No	S6
Electrochemical immunoassay	Ag^{+}@CTAB–AuNPs	–	0.0655 ng mL^{-1}	No	S7
Fluorescence	Eu(TATB)	4.598×10^4	0.67 μM	Yes	S8
Fluorescence	$[Tb(L)(H_2O)_2 \cdot 3H_2O]_n$	1.38×10^3	1.43 ppm	–	S9
Fluorescence	$[Cd_2(L)_2(bib)(H_2O)_2]$	2.98×10^3	1.05 ppm	No	S10
Fluorescence	$\{Eu(BTB)DMF\}_n$	4.60×10^4	0.65 μM	Yes	S11
Fluorescence	$[Zn(oba)_2(bpy)_2]$	1.13×10^4	–	No	S12
Fluorescence	$[Co_2(OH)(H_2O)_2(cbca).2H_2O]_n$	2.39×10^4	0.68 μM	No	S13
Fluorescence	$[Zn(DTP)SO_4(H_2O)_3]$	3.70×10^4	0.25 μM	No	S14
Ratiometric fluorescence	**3**	1.15×10^4	0.62 μM	Yes	This work

Table S6. Luminescent lifetimes of **3** before and after sensing SMZ in aqueous solutions.

MOFs	solution	τ_{before} (μs)	τ_{after} (μs)
3	aqueous solution	18.8	18.6

Table S7. Colour coordinates of **1–9** according to CIE 1931 with varied quantum yields

Compounds	CIE (x, y)	Quantum yield	Color
Eu (**1**)	(0.577, 0.382)	13.83%	red
Gd (**2**)	(0.167, 0.116)	6.60%	blue
Tb (**3**)	(0.336, 0.534)	3.76%	green
$Tb_{0.98}Eu_{0.02}$ (**4**)	(0.410, 0.491)	18.38%	yellow–green
$Tb_{0.96}Eu_{0.04}$ (**5**)	(0.468, 0.440)	17.82%	yellow
$Tb_{0.94}Eu_{0.06}$ (**6**)	(0.519, 0.400)	19.83%	orange
$Gd_{0.94}Eu_{0.06}$ (**7**)	(0.466, 0.303)	17.68%	pink
$Gd_{0.96}Tb_{0.04}$ (**8**)	(0.222, 0.242)	25.20%	light blue
$Gd_{0.95}Tb_{0.03}Eu_{0.02}$ (**9**)	(0.348, 0.322)	11.39%	white

Table S8. Summary of the quantum yields of the reported white–light–emission doped MOFs.

Compounds	Quantum yield	Ref.
$La_{0.6}Eu_{0.1}Tb_{0.3}$–BTPCA	47.33 %	S15
$Eu_{0.0855}Gd_{0.6285}Tb_{0.2860}$	22.4 %	S16
$Eu_{0.045}Tb_{0.955}$CPOMBA	15 %	S17
$La_{0.6}Eu_{0.1}Tb_{0.3}$CPOMBA	14.4 %	S17
HMA–$Tb_{10}Eu_1$	11.41 %	S18
0.5%Eu^{3+}–doped 2–Tb	11.4 %	S19
$Gd_{0.95}Tb_{0.03}Eu_{0.02}$	11.39%	This work
ZJU–1:1.0%Tb^{3+}, 2.0%Eu^{3+}	6.11 %	S20
ZJU–1:1.5%Tb^{3+}, 2.0%Eu^{3+}	6.80 %	S20

Reference

S1. H. Xu, H. Zhou, L. Feng, Q. Wang, R. Chen, W. Huang, X. Wu, Synthesis, crystal structures, and magnetic properties of six transition metal phosphonates, *Dalton Trans*., 2018, **47**, 11226–11238.

S2. M. J. Frisch, G. W. Trucks, H. B. Schlegel, G. E. Scuseria, M. A. Robb, J. R. Cheeseman, G. Scalmani, V. Barone, B. Mennucci, G. A. Petersson, H. Nakatsuji, M. Caricato, X. Li, H. P. Hratchian, A. F. Izmaylov, J. Bloino, G. Zheng, J. L. Sonnenberg, M. Hada, M. Ehara, K. Toyota, R. Fukuda, J. Hasegawa, M. Ishida, T. Nakajima, Y. Honda, O. Kitao, H. Nakai, T. Vreven, J. A. Jr. Montgomery, J. E. Peralta, F. Ogliaro, M. Bearpark, J. J. Heyd, E. Brothers, K. N. Kudin, V. N. Staroverov, R. Kobayashi, J. Normand, K. Raghavachari, A. Rendell, J. C. Burant, S. S. Iyengar, J. Tomasi, M. Cossi, N. Rega, J. M. Millam, M. Klene, J. E. Knox, J. B. Cross, V. Bakken, C. Adamo, J. Jaramillo, R. Gomperts, R. E. Stratmann, O. Yazyev, A. J. Austin, R. Cammi, C. Pomelli, J. W. Ochterski, R. L. Martin, K. Morokuma, V. G. Zakrzewski, G. A. Voth, P. Salvador, J. J. Dannenberg, S. Dapprich, A. D. Daniels, O. Farkas, J. B. Foresman, J. V. Ortiz, J. Cioslowski, D. J. Fox, Gaussian 09, Revision A. 02.

S3. O. V. Dolomanov, L. J. Bourhis, R. J. Gildea, J. A. K. Howard, H. Puschmann, OLEX2: a complete structure solution, refinement and analysis program, *J. Appl. Crystallogr.*, 2009, **42**, 339–341.

S4. P.S. Peixoto, I.V. Tóth, S. Machado, L. Barreiros, A. Machado, A.A. Bordalo, J.L.F.C. Lima, M.A. Segundo, Screening of sulfonamides in waters based on miniaturized solid phase extraction and microplate spectrophotometric detection, *Anal. Methods.*, 2018, **10**, 690–696.

S5. Y. Wang, X. Yan, Q. Kou, Q. Sun, Y. Wang, P. Wu, L. Yang, J. Tang, T. Le, An Ultrasensitive Label–Free Fluorescent Aptasensor Platform for Detection of Sulfamethazine, *Int. J. Nanomedicine.*, 2021, **16**, 2751–2759.

S6. L. Ouyang, L. Zhu, Y. Ruan, H. Tang, Preparation of a native β–cyclodextrin modified plasmonic hydrogel substrate and its use as a surface–enhanced Raman scattering scaffold for

antibiotics identification, *J. Mater. Chem. C.*, 2015, **3**, 7575–7582.

S7. M. Yang, X. Wu, X. Hu, K. Wang, C. Zhang, E. Gyimah, S. Yakubu, Z. Zhang, Electrochemical immunosensor based on Ag^{+}–dependent CTAB–AuNPs for ultrasensitive detection of sulfamethazine, *Biosens. Bioelectron*., 2019, **144**, 111643.

S8. K. Ren, S. H. Wu, X. F. Guo, and H. Wang, Lanthanide Organic Framework as a Reversible Luminescent Sensor for Sulfamethazine Antibiotics, *Inorg. Chem*., 2019, **58**, 4223–4229.

S9. G. Li, T. Wang, S. H. Zhou, J. W, H. Lv, M. L. Han, D. P, Singh, A. Kumar e, J. C. Jin, New highly luminescent 3D Tb(III)–MOF as selective sensor for antibiotics, *Inorg. Chem. Commun.*, 2021, **130**, 108756.

S10. C. C. Shi, L. Zhao, J. J. Xu, L. Lu, A. Singh,· O. Prakash, A. Kumar, New Three–dimensional Supramolecular Cd(II)–Coordination Polymer as a Luminescent Sensor for Sulfamethazine Detection, *J. Inorg. Organome. P.*, 2022, **32**, 4627–4636.

S11. K. Ren, S. H. Wu, X. F. Guo, H. Wang, Lanthanide organic framework as a reversible luminescent sensor for sulfamethazine antibiotics, *Inorg. Chem.*, 2019, **58**, 4223–4229.

S12. P. P. Guo, M. Liu, L. L. Shi, A Zn–based coordination polymer as a luminescent sensor for simple and sensitive detecting of sulfonamides antibiotics and nitroaromatic, *J. Solid. State. Chem.*, 2020, **286**, 121247.

S13. B. L. Li, J. K. Wang, J. S. Gao, Y. H. Yu. D. S. Ma, A semi–rigid tricarboxylate ligand based Co(II) coordination polymer: construction and applications in multiple sensing, *New. J. Chem.*, 2020, **44**, 3664.

S14. B. Y. Yu, D. Wang, G. S. Zhu, C. J. Wei, Y. Jia, C. L. Song, J. Cheng, H. Q. Zhao, Synthesis, crystal structure of four 1D to 3D coordination polymers and potential sensor for the detection

of ions, antibiotics and pesticides in water media, *Polyhedron.*, 2023, **230**, 116242.

S15. Q. Tang, S. Liu, Y. Liu, D. He, J. Miao, X. Wang, Y. Ji, Z. Zheng, Color Tuning and White Light Emission via in Situ Doping of Luminescent Lanthanide Metal–Organic Frameworks, *Inorg. Chem.*, 2014, **53**, 289–293.

S16. X. Y. Li, W. J. Shi, X. Q. Wang, L. N. Ma, L. Hou, Y. Y. Wang, Luminescence Modulation, White Light Emission, and Energy Transfer in a Family of Lanthanide Metal−Organic Frameworks Based on a Planar π–Conjugated Ligand, *Cryst. Growth Des.*, 2017, **17**, 4217–4224.

S17. Y. Zhao, F. Zhang, X. Zhang, Single Component Lanthanide Hybrids Based on Metal–Organic Framework for Near–Ultraviolet White Light LED, *ACS Appl. Mater. Interfaces*., 2016, **8**, 24123–24130.

S18. H. Liu, T. Chu, Z. Rao, S. Wang, Y. Yang, W. Wong, The Tunable White–Light and Multicolor Emission in an Electrodeposited Thin Film of Mixed Lanthanide Coordination Polymers, *Adv. Opt. Mater.*, 2015, **3**, 1545–1550.

S19. Z. Liu, M. Wu, S. Wang, F. Zheng, G. Wang, J. Chen, Y. Xiao, A. Wu, G. Guo, J. Huang, Eu^{3+} –Doped Tb^{3+} Metal–Organic Frameworks Emitting Tunable Three Primary Colors Towards White Light, *J. Mater. Chem. C.*, 2013, **1**, 4634–4639.

S20. X. Rao, Q. Huang, X. Yang, Y. Cui, Y. Yang, C. Wu, B. Chen, G. Qian, Color Tunable and White Light Emitting Tb^{3+} and Eu^{3+} Doped Lanthanide Metal–Organic Framework Materials. *J. Mater. Chem.*, 2012, **22**, 3210–3214.